

1 INTRODUCTION

Telescopes in space allow science in wavelength bands absorbed by Earth's atmosphere, avoid atmospheric distortion, provide a stable environment with low infrared background noise, and permit long integration times.¹ However, cost is a significant driver. Ground-based optical telescopes are currently being designed with segmented primary mirror diameters of 30 m (using 492 segments)² and 42 m (984 segments).³ In contrast, the 18-segment primary mirror of the James Webb Space Telescope (JWST)⁴ is 6.5 m, and future designs for the Advanced Technology Large Aperture Space Telescope (ATLAST) range from a monolithic 8 m mirror to segmented 9.2 and 16.8 m designs,¹ all significantly smaller than what can be achieved at much lower cost on the ground. The goal herein is to propose active control of the mirror segments as a key enabler for building much larger diameter telescopes in space.

A key driver limiting affordable aperture sizes in space is the primary mirror mass or areal density, with the JWST and ATLAST segmented mirrors being of order 25 kg/m² (including required support structure mass). In contrast, actuated hybrid silicon carbide mirror segments have been proposed⁵ with areal densities <10 kg/m², as low as 3 kg/m² using 1 mm thick silicon segments,⁶ and potentially even thinner and lighter with internal actuation.⁷ However, highly segmented space telescope designs such as that presented in [6] (using ~0.3 m diameter segments) have not included controls analysis, and the aim here is to illustrate that the resulting large numbers of segments (e.g. 12 000 for a 30 m mirror) can be robustly controlled. There are of course additional design and manufacturability issues regarding the segments, actuation, and sensing. Highly-segmented concepts have also been introduced for ground-based telescopes,⁸ and other space telescope designs with of order 1000 segments have also been proposed.⁹ Membrane-based approaches have also been suggested for large lightweight space telescopes (see e.g. the review by Santer and Seffen¹⁰), however, these may also require somewhat similar controls technology to provide adequate optical surface quality.

43 The total mass of the JWST telescope (not including instrumentation or spacecraft bus)
44 is roughly 4 times larger than the mass of the primary mirror, and thus it is insufficient to
45 address only the areal density of the mirror and not also develop a strategy to minimize
46 structural mass. Thus while some mechanical interface is required between neighboring
47 segments to provide in-plane stiffness, providing a stiff back-support structure would defeat
48 the purpose of minimizing mirror areal density. Minimizing structural mass results in a
49 mirror that is highly flexible in its optically-relevant out-of-plane motion, and active surface
50 control will be required: even though there are few disturbances in space, some stiffness is
51 required to enable repointing of the telescope in reasonable time. Thus the control problem
52 involves thousands of actuators and sensors, and thousands of lightly-damped structural
53 modes within the control bandwidth. A solution for this problem has recently been proposed
54 in the context of large (1-3 m) deformable mirrors for ground-based adaptive optics.^{11,12}
55 The first observation is that it is always possible to implement collocated rate feedback
56 with some minimum but finite bandwidth (i.e., with realistic actuators and sensors) due
57 to the high modal density. Second, collocated control guarantees robustness but does not
58 provide adequate stiffness for low spatial-frequency deformations, while feedback of global
59 sensor information provides performance but poor robustness. The proposed strategy uses
60 only local information to yield performance near that of a global solution, while retaining
61 robustness by not relying on global information. No claim is made regarding optimality, but
62 simply a demonstration of feasibility.

63 While the objective here is to demonstrate that a large array of segments can be con-
64 trolled, and not to provide a detailed point design of a telescope using these ideas, a gen-
65 eral description is useful for defining design constraints (section II). The remaining sections
66 develop the telescope model (section III), and develop and demonstrate the local control
67 (section IV).

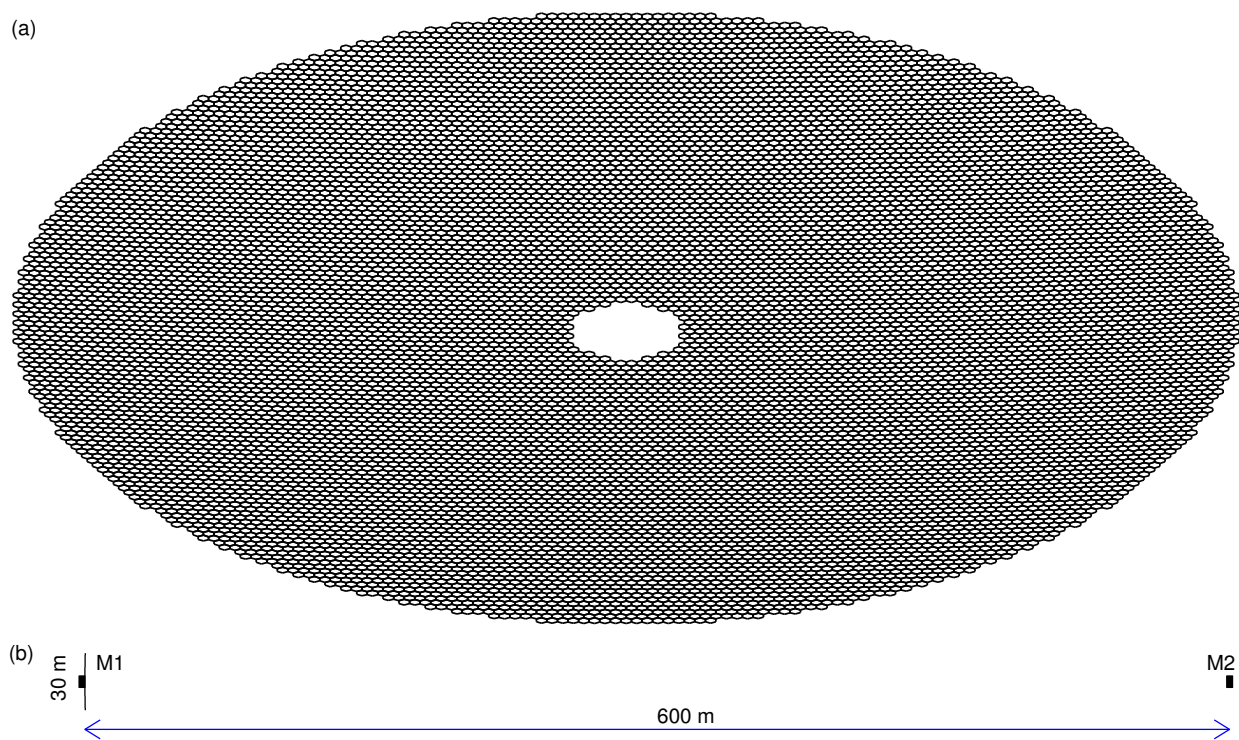


Figure 1: (a) Schematic of a 12 000 segment mirror (viewed from a 30° elevation angle), with hexagonal segment diameter 1% of the mirror diameter (e.g., 30 m with 0.3 m segments). The secondary mirror (M2) would be on a separate formation-flying spacecraft, as shown in (b) with the primary mirror (M1) to scale.

2 CONCEPT

Science cases for future large-aperture optical and near-IR space telescopes are described, for example, in [1]. One motivator for such a facility would be the capability for assessing the potential for life on Earth-like planets of other stars. The larger the aperture, the greater number of star systems can be considered, both because more light-gathering capability means less integration time, and because higher resolution allows distinguishing star-light from planet at greater distances from the Earth. For this type of science, the overall field-of-view would not need to be very large. Sufficient integration time is required for spectroscopic measurements to understand atmospheric composition, while the total number of targets to be evaluated by the facility during its lifetime might be only a few thousand. For this mission, then, it may be acceptable if it takes many hours to change the orientation of the telescope to point at a different target, but a settling time of days would impact the science mission. For the simulation parameters described in the next section, the first resonant frequency of a 30 m primary mirror is ~ 0.1 Hz; with damping as low as 0.1%, the uncontrolled settling time to a few nm residual error from a 90° degree slew manoeuvre would be of order a day.

The key innovation herein is thus a strategy that enables control of a highly-segmented filled-aperture primary mirror. An example is illustrated in Fig. 1, with $N = 12\,000$ hexagonal segments with maximum radius 0.15 m (as in [6]). Mass is minimized both by (i) reducing segment size so that segment thickness can be reduced, without requiring additional degrees of freedom of actuation internal to the segment for shape control, and (ii) minimizing the mechanical interconnections between segments. In-space assembly, either robotic or with astronauts, is plausible if the interconnection tasks are straightforward,^{9,13,14} and if control can be used to correct errors resulting from not having a precision deployable structure.⁵

The mechanical interface between neighbouring segments provides stiffness for the in-plane degrees of freedom of the segment array, but does not need to provide significant stiffness for the out-of-plane degrees of freedom, since these will need to be actively controlled.

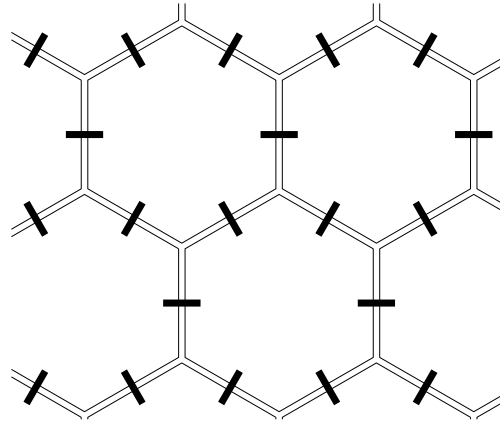


Figure 2: Detail on segmentation geometry (with gaps enlarged for clarity), using a single mechanical interconnection between neighbouring segments. The interconnection must be lightweight and designed for ease of assembly. Its primary purpose is to provide in-plane stiffness, but it will also provide some stiffness to both relative out-of-plane segment motion and relative dihedral angle change between segments. Two degrees of freedom of actuation provide both relative force and torque.

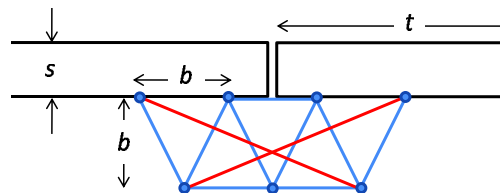


Figure 3: Sketch of mechanical interconnect between neighboring segments used to estimate representative stiffness values in simulation. The long diagonals (red) are active members to apply differential force/torques between segments; the truss provides differential translational and rotational stiffness between neighboring segments. The dimension b is chosen so that the interconnect structure could be folded behind a segment during launch.

94 A single interface between segments, as shown in Fig. 2, simplifies assembly, but requires
95 that the interface provide stiffness and actuation authority for both relative out-of-plane
96 inter-segment motion and inter-segment dihedral angle. (Note that with only a single degree
97 of freedom per inter-segment edge, there would not be enough actuators to constrain the
98 $3N$ degrees of freedom of the full segment array; with two degrees of freedom per edge there
99 are more actuators than required to control segment rigid-body motion.) It is also possible
100 to use two interconnects;⁶ the relative advantages are unclear without more detail design,
101 including consideration for both actuation and assembly. The single interconnect approach
102 is used herein, with nominal stiffness parameters based on the sketch in Fig. 3.

103 In addition to eliminating the structural weight supporting the primary mirror (M1),
104 there is no need for structure between the primary and secondary mirror (M2) if formation
105 flying is used for the M2 subsystem, as suggested in [6, 15] (and plausible if repointing of the
106 telescope is not frequent). This also means that the primary focal-length of the telescope is
107 not driven by structural weight or launch-packaging considerations, but only by the optical
108 design; [15] proposes a focal-ratio of 20 so that for a 30 m primary mirror, M2 would be
109 0.6 km away. A consequence of long focal lengths and many segments is that the segment
110 surface can be spherical rather than hyperbolic, and hence the segments can be identical; this
111 is essential for minimizing manufacturing cost and also reduces the complexity of in-space
112 assembly. The overall M1 shape may still be parabolic or hyperbolic, and optical distortion
113 may be improved with the ability to statically adjust the radius of curvature of each segment;
114 the required adjustment decreases as the segment size decreases. As in [15], sun-shades can
115 also be separate satellites flown in formation. Formation flying requires that the telescope
116 not be in Earth orbit with its gravity-gradient torques, but at one of the stable Lagrange
117 points (as JWST).

118 The mass of the spacecraft bus and instrumentation, located in the central obscuration
119 of the primary mirror, will be significant, but does not scale with collecting area.

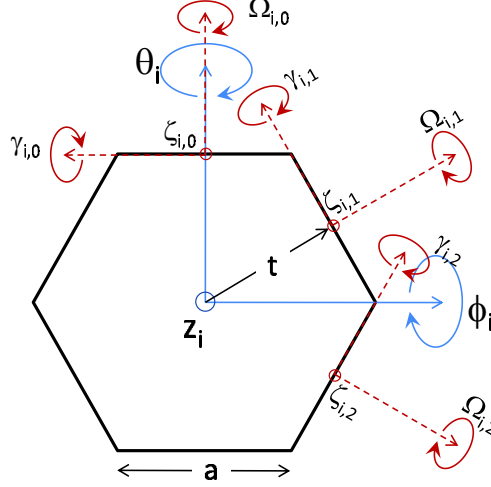


Figure 4: Segment coordinate system z_i , θ_i , ϕ_i (blue) and rotated coordinate systems $\zeta_{i,k}$, $\gamma_{i,k}$, $\Omega_{i,k}$ (red) at the interface point with the neighbouring segment in the k^{th} direction. a is the segment radius or side length, $t = a\sqrt{3}/2$ is the radius at the interconnection points. Actuators at 3 of the 6 interconnection points are numbered with that segment, and the other 3 with the relevant neighbour.

120 3 MODEL

121 Since the in-plane segment motions are passively constrained by the mechanical intercon-
 122 nection, only the three out-of-plane degrees of freedom need to be included in the dynamic
 123 model; here we describe the motion using segment piston (z) and rotations (Fig. 4) so
 124 $x_i = [\phi_i \ \theta_i \ z_i]^T$, and the generalized displacement vector $x = [x_1^T \cdots x_N^T]^T$ satisfies

$$M\ddot{x} + D\dot{x} + Kx = \Phi f \quad (1)$$

125 For ease of calculation, an extra coordinate system (Fig. 4) is introduced for each con-
 126 nection point $k = 0, \dots, 5$ on segment i :

$$\begin{pmatrix} \Omega_{i,k} \\ \gamma_{i,k} \\ \zeta_{i,k} \end{pmatrix} = R_k x_i \quad (2)$$

127 where

$$R_k = \begin{pmatrix} \sin(k\pi/3) & \cos(k\pi/3) & 0 \\ -\cos(k\pi/3) & \sin(k\pi/3) & 0 \\ t \cos(k\pi/3) & -t \sin(k\pi/3) & 1 \end{pmatrix} \quad (3)$$

128

129 The stiffness and damping forces created in the connection joints will influence all three
 130 of its local coordinates, although the contribution in the Ω direction will be weak and could
 131 be ignored. Sufficient actuation degrees of freedom require only a force, F , and torque, M ,
 132 corresponding to directions ζ and γ . Neglecting damping, the equations of motion for each
 133 segment can then be written as

$$\begin{aligned} M_s \ddot{x}_i + \sum_{k=0}^5 R_k^T K_s \left[\begin{pmatrix} \Omega_{i,k} \\ \gamma_{i,k} \\ \zeta_{i,k} \end{pmatrix} + \begin{pmatrix} \Omega_{i(k),k+3} \\ \gamma_{i(k),k+3} \\ -\zeta_{i(k),k+3} \end{pmatrix} \right] \\ = \sum_{k=0,2,4} K_{FX} \begin{pmatrix} F_{i,k} \\ M_{i,k} \end{pmatrix} + \sum_{k=1,3,5} K_{FX} \begin{pmatrix} -F_{i(k),k} \\ M_{i(k),k} \end{pmatrix} \end{aligned} \quad (4)$$

134 where the relevant stiffness and actuation contributions are not included at boundary seg-
 135 ments, and

$$M_s = \begin{pmatrix} J_\phi & 0 & 0 \\ 0 & J_\theta & 0 \\ 0 & 0 & m_s \end{pmatrix} \quad (5)$$

136

$$K_s = \begin{pmatrix} K_\Omega & 0 & 0 \\ 0 & K_\gamma & 0 \\ 0 & 0 & K_\zeta \end{pmatrix} \quad (6)$$

137

$$K_{FX} = \begin{pmatrix} t \cos(k\pi/3) & -\cos(k\pi/3) \\ -t \sin(k\pi/3) & \sin(k\pi/3) \\ 1 & 0 \end{pmatrix} \quad (7)$$

138 The notation $j = i(k)$ above refers to the segment j which borders segment i at orientation
139 k .

140 The equations of motion are sparse; to preserve this, damping is added of the form
141 $D = c_1 M + c_2 K$, with c_1 and c_2 chosen to give 0.1% damping at the first resonance and at
142 500 Hz.

143 The spacecraft bus and instrumentation in the center of the mirror will have significant
144 mass M_{center} . The model assumes that the bus is connected to the neighbouring segments
145 with the same mechanical interconnection as between any other pair of segments. The
146 internal flexibility of the bus is ignored.

147 For the purposes of illustrating the control concept, consider silicon carbide segments,
148 $s = 1$ mm thick with maximum radius $a = 15$ cm. Representative values for the stiffness
149 of the mechanical interconnection between segments are obtained by analyzing the truss
150 structure in Fig. 3; this is only to obtain reasonable parameter estimates and not to propose a
151 specific design. The mass of each mechanical interconnect is assumed to be 10% of the mass of
152 the SiC segment (so the total mechanical mass adds 30% to the mass). The depth influences
153 the stiffness; this is chosen to be a fraction of the segment radius to allow a design that
154 folds into the back of the segment for launch. This yields the stiffness parameters in Table 1.
155 For analysis, the mechanical interconnections, actuators, sensors, and electronics/cabling are
156 assumed to increase the mass $\rho s = 2.95$ kg/m² of the SiC alone by 50% without altering the
157 mass distribution. Thus with $\mu = 1.5$, the segment mass and moment of inertia is

$$m = \mu \frac{3\sqrt{3}}{2} \rho s a^2 \quad J_\theta = J_\phi = \mu \frac{5\sqrt{3}}{16} \rho s a^4 \quad (8)$$

Parameter	Value	Parameter	Value
ρ	$2.95 \times 10^3 \text{ kg/m}^3$	K_Ω	10
a	0.15 m	K_γ	4.2e3 Nm/rad
s	1 mm	K_ζ	3.7e6 N/m
b	0.04 m	M_{center}	4000 kg
N	12000	J_{center}	3100 kg m ²

Table 1: Parameters used in simulation.

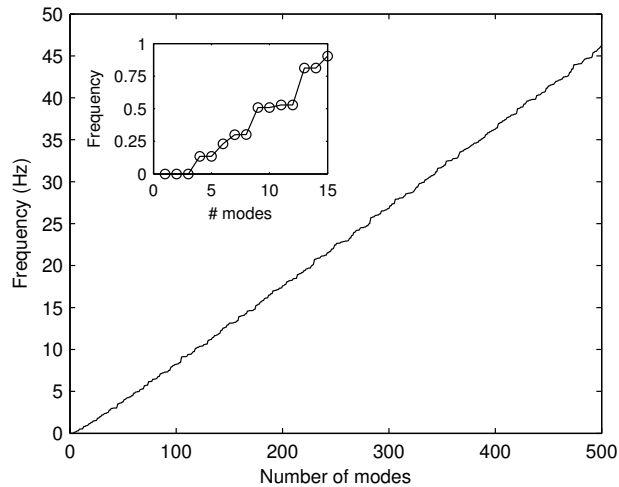


Figure 5: First 500 resonant frequencies of a 30m mirror using the segment parameters in Table 1. The modal density is roughly constant with frequency, at slightly more than 10 modes per Hertz. The inset shows the first 15 modes.

158 For the purpose of understanding the low spatial/temporal frequency modes of the overall
159 mirror, the flexibility of an individual segment can be ignored. Using these parameters, the
160 first resonance of a segment will be of order 1 kHz. The modal density of the mirror array,
161 without internal segment modes, is roughly constant, shown in Fig. 5. The first flexible
162 mode is at 0.13 Hz, and there are 14 flexible modes below 1 Hz.

163 4 CONTROL

164 4.1 Control problem

165 There are $3N$ controlled degrees of freedom for the overall segmented-mirror (the in-plane
 166 degrees of freedom are passively controlled by the mechanical interconnection), and slightly
 167 less than $6N$ degrees of freedom of relative actuation. The extra degrees of freedom could
 168 either be constrained to be zero (as here), or used to provide small deformations of the
 169 segments to modify their radius of curvature in both the radial and azimuthal directions.

170 Two sensors are also needed on each edge to measure the relative motion between seg-
 171 ments. A similar approach has been proven on ground-based segmented-mirror telescopes,
 172 with resolution of a few nm using either differential capacitive or differential inductive sen-
 173 sors. Unless a manufacturing approach is used that ensures sensor installation errors of
 174 nanometers, an initial phasing approach using starlight would be needed after the mirror
 175 was assembled in order to determine the correct set-point for each sensor; these techniques
 176 are well established on the ground but some modifications to the approach would be required
 177 to handle many thousands of segments.⁵ Having mechanical edge sensors means that optical
 178 feedback is not continuously required, except for low-order mirror deformations that are not
 179 well observed by relative measurements between segments.

180 The transformation between segment motion and sensor response can be determined from
 181 geometry.¹⁶ The global piston, tip and tilt of the entire mirror cannot be measured with
 182 internal relative sensor measurements (nor controlled with relative actuators), aside from
 183 these degrees of freedom the transformation is invertible. However, while the transformation
 184 from motion to sensor response is sparse, the inverse is in general fully populated; that is,
 185 the estimation of segment motion requires global knowledge. For ground-based segmented-
 186 mirrors, where the actuators influence the absolute motion of the segments, the inverse
 187 transformation has been shown to require attention to robustness (which is challenging¹⁷)

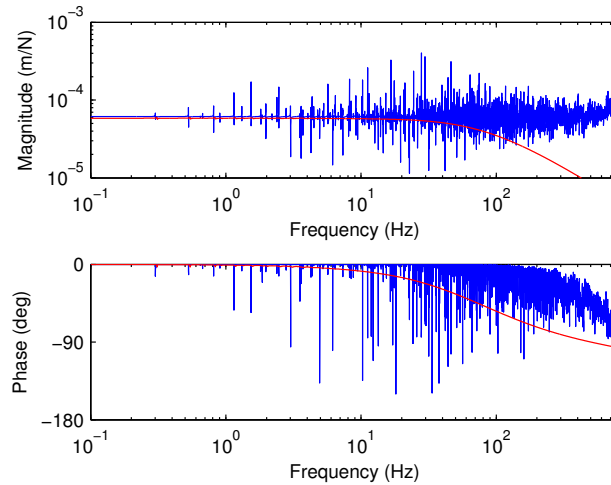


Figure 6: Representative collocated transfer function for a force actuator, without (blue) and with (red) active damping. With no added damping, the phase varies between 0 and -180° at moderate frequency, but the variation in phase and magnitude become smaller above roughly 500 Hz where the half-power bandwidth of each mode becomes larger than the modal spacing. The curve with active damping diverges from the uncontrolled case at high frequency because the damping parameters are chosen so that the high frequency modes are overdamped (yielding real rather than complex poles).

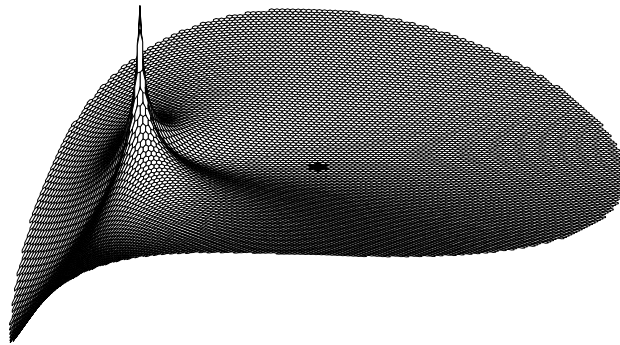


Figure 7: Static response pattern for a torque command on a representative actuator (magnified); the influence pattern is non-local.

188 and to computation (which is solvable^{18,19}). With actuation that influences only relative
 189 motion between segments, there is a related problem of finding the set of actuator commands
 190 that produces a desired segment motion. Here the focus is on dynamics (in Sec. 4.2), and
 191 on this actuator distribution problem (in Sec. 4.3), and it is assumed that the estimation
 192 problem is solvable using previously developed techniques.

193 Fig. 6 and 7 illustrate representative characteristics of the mirror, including the transfer
194 function between a representative actuator and the collocated response, and the static re-
195 sponse shape of the mirror resulting from a unit command on a representative actuator. The
196 two foci noted above are related to the behavior in these two figures. The first challenge is the
197 ability to add active damping despite the presence of many modes both within and above the
198 control bandwidth (i.e. compensating for the behavior in Fig. 6). Realistic actuator/sensor
199 dynamics preclude arbitrarily high bandwidth and roll-off will be required at some frequency.
200 The second challenge is the ability to manage the wide range of spatial scales introduced
201 by actuation without requiring global knowledge that would inevitably limit robustness (i.e.
202 compensating for the resonant behavior in Fig. 7). Approaches for these key challenges are
203 described in Sections 4.2 and 4.3 below.

204 4.2 Collocated control

205 The relative motion collocated with the actuators can be obtained from sensors between
206 neighboring segments, using only a local transformation. Using this information, collocated
207 rate feedback can add significant damping, making the position control design more straight-
208 forward. While this is guaranteed to be robustly stable, in practice rate feedback has finite
209 bandwidth due to sensor and actuator dynamics and electronic implementation. While the
210 simulation here has a highest resonant frequency ~ 1.5 kHz, the real mirror will have higher
211 frequency resonances due to internal segment dynamics. However, above some frequency, the
212 half-power bandwidth of the structural modes will exceed the modal spacing, leading to a
213 relatively smoother transfer function in both magnitude and phase;¹¹ see Fig. 6. Practically,
214 this means that active damping is feasible provided it has a minimum bandwidth. The high
215 number of modes in this problem means that this “acoustic limit” for the structural behav-
216 ior is at a low enough frequency that active damping is plausible with realistic actuator and
217 sensor bandwidths (less than 1 kHz).

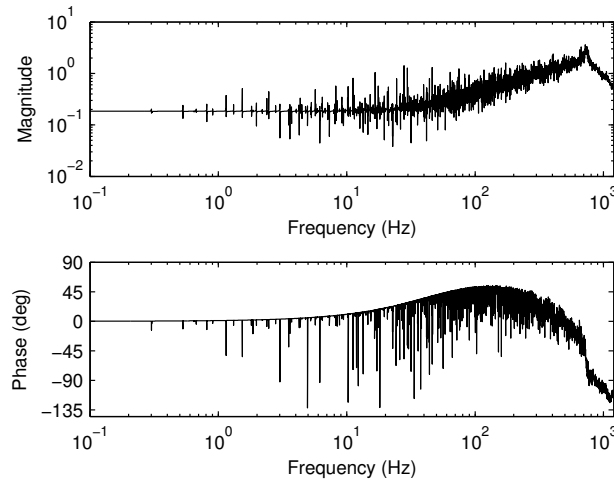


Figure 8: Representative collocated loop transfer function for a force actuator. Roll-off is introduced at high frequencies, but because the phase variations are small, the control remains stable. In addition to the active damping, a small position feedback adds some stiffness.

218 Collocated position feedback behaves as an electronic spring, and is similarly guaranteed
 219 to be stable, but with negligible phase margin if the gain is large enough to have a significant
 220 effect (loop gain larger than one). A small, stable, position gain is used in the simulations
 221 here, which has a small stiffening effect on the lowest frequency modes.

222 The average slope of the transfer function from force to collocated displacement, or torque
 223 to collocated rotation, is roughly zero (a constant; Fig. 6), and thus rate feedback has higher
 224 loop gain at higher frequency, and thus adds more damping to higher frequency modes than
 225 to low. A high rate feedback gain is chosen here that results in over-damping many of the
 226 high frequency modes in order to provide some damping to the lower frequency modes. Note
 227 that even adding a small amount of damping at each collocated actuator/sensor pair can
 228 result in significant total damping due to the large number of actuators. Including both rate
 229 and position feedback, the collocated loop transfer function for a representative actuator is
 230 shown in Fig. 8, and the resulting closed-loop transfer function shown in Fig. 6. The added
 231 damping yields a more straightforward problem for an outer control loop.

232 4.3 Local feedback

233 As illustrated by the static response pattern in Fig. 7, the control has much higher gain on
 234 low spatial-frequency deflection patterns than on high (that is, the plant is ill-conditioned).
 235 A collocated strategy means that in response to a particular non-zero inter-segment motion,
 236 the control will apply solely the corresponding relative actuator command, giving a global
 237 response to a local error. A global feedback strategy could readily avoid this, by inverting
 238 the system dynamics, at the expense of requiring, and hence being dependent on, both global
 239 model knowledge and global state information. The innovation used herein is to use only
 240 local actuation in response to a particular segment displacement; this provides a remarkably
 241 good compromise between performance and required knowledge.^{11,12} Because the collocated
 242 control described above suppresses much of the dynamic variation, it is sufficient to develop
 243 an approximate local inverse that is valid quasi-statically.

244 The resulting architecture is shown in Fig. 9. $G(s)$ is the plant dynamics from actuator
 245 input to collocated sensor output (including any required local transformation from sensor to
 246 equivalent collocated response). The matrix B describes the problem of estimating segment
 247 positions from relative sensor information; this has received attention in the context of
 248 ground-based telescopes, and is not discussed here. The remainder of this section describes
 249 the construction of the matrix Q that provides a sparse, local approximate static inverse to
 250 BG , so that $BG(0)Q \simeq I$; Q takes desired segment position commands x_d and generates
 251 an actuator distribution that approximately matches x_d without requiring forces throughout
 252 the entire mirror.

253 Define the set Ω_k of actuators local to segment k . For illustration here, Ω_k is chosen to
 254 include all actuators on both segment k and every immediately adjacent segment, for a total
 255 of 60 (out of 72000) actuators for an interior segment. The number of actuators used in
 256 each set is a design choice that trades nominal performance with increased complexity and
 257 decreased robustness; this ultimately needs to be made based on specific design requirements.

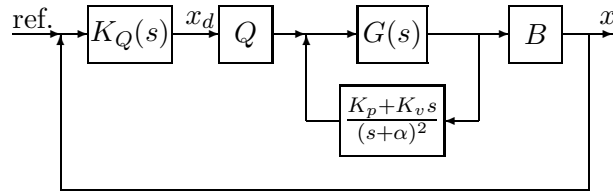


Figure 9: Block diagram of control system. $G(s)$ is the open-loop system with 36 000 degrees of freedom and nearly 72 000 actuators. Collocated rate feedback K_v adds damping, position gain K_p adds stiffness, but both are limited by actuator and sensor dynamics represented above by poles at $s = -\alpha$. The outer position control loop is made better conditioned using the matrix Q ; this is sparse and local, and provides an approximate inverse to the static plant.

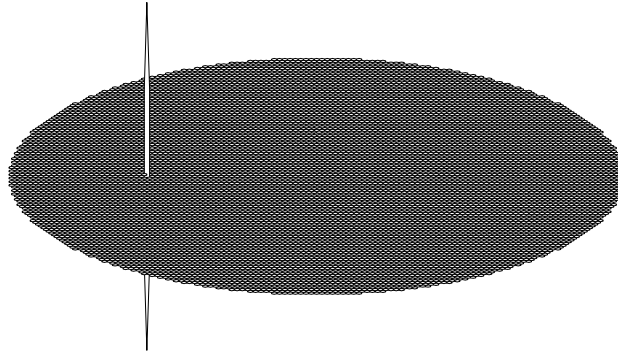


Figure 10: Static response pattern for a command to a representative local family group in response to a desired single segment rotation; compare with Fig. 7. The response away from the segment is negligible.

258 Increasing the size of the local region will result in improved suppression of more modes in
 259 the local control loop.¹²

260 Referring to eq. (1), the static response of the mirror to an actuator command f is $x =$
 261 $C\Phi f$, where $C = K^\#$ is a modified compliance matrix, where the uncontrollable rigid body
 262 modes are projected out (C is the pseudo-inverse of K , note that eigenvectors corresponding
 263 to zero eigenvalues of K are also uncontrollable). C is fully-populated and ill-conditioned.

264 Define the vector e_{ki} to be a unit displacement of coordinate i on segment k , and choose

265 the actuator response pattern f_{ki} that minimizes the cost function

$$J = \|C\Phi f_{ki} - e_{ki}\|_2 \quad (9)$$

266 subject to the constraint that elements of the vector f_{ki} not in the set Ω_k must be zero.
 267 That is, choose a local set of forces to minimize the rms error over the entire mirror in
 268 matching the displacement pattern. The constrained least-squares problem is equivalent to
 269 solving an unconstrained problem with a truncated matrix $\Psi_k = C\Phi_{:, \Omega_k}$ where only the
 270 columns of Φ associated with actuators in Ω_k are retained. The row of the pseudo-inverse of
 271 Ψ_k corresponding to the i^{th} coordinate on the k^{th} segment gives the appropriate local force
 272 distribution f_{ki} to compensate for an error at location k . Assembling, for each k and i , the
 273 resulting pattern into a matrix Q (so $Q_{\Omega_k, ki} = f_{ki}$), then Q gives an approximate inverse to
 274 the system at zero frequency, based on local actuation only. Control can then be based on
 275 Qx rather than collocated control. This approach is identical in derivation to that in [11],
 276 and motivated by the local approach used in [20] to develop computationally efficient sparse
 277 reconstructor matrices for adaptive optics estimation. The resulting response distribution
 278 to a single segment rotation error is shown in Fig. 10; the response to a position error is
 279 similarly local.

280 A representative transfer function between an input to a single local actuator group and
 281 the resulting segment response is shown in Fig. 11; since Q is an approximate static inverse
 282 of the plant, the resulting system is decoupled and normalized to unit gain at zero frequency.
 283 With this (static) transformation between segment position errors and the appropriate cor-
 284 responding force distribution, it is much more straightforward to design a position controller.
 285 The resulting closed-loop performance with a low-bandwidth control is shown in Fig. 12.

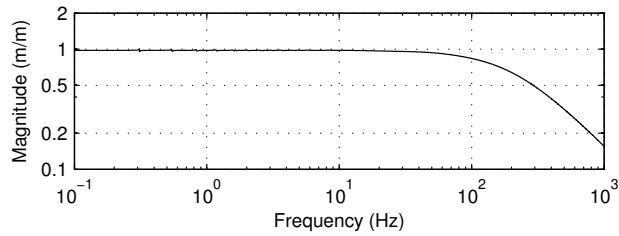


Figure 11: Representative transfer function from an input to a local force distribution to the resulting segment position response (from one element of x_d to the corresponding element of x in Fig. 9). In addition to the modes of the system being well damped, the system dynamics are normalized so that the low- and high-spatial frequency gains are comparable. The cross-coupling to other displacements on the same segment are a factor of 10^4 smaller.

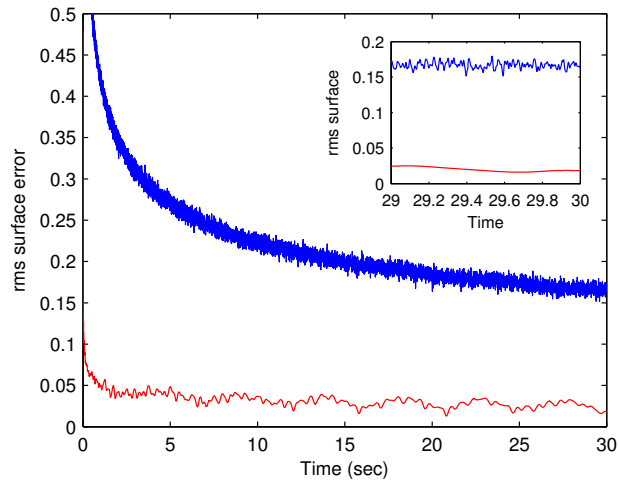


Figure 12: Time history of root-mean-square surface response from a random initial condition, open-loop (blue) and closed-loop (red). The highest spatial frequencies in the open-loop model are quickly damped due to the assumed non-modal damping, leaving a broad range of spatial- and temporal-frequencies in the response (shown more clearly in the inset). The closed-loop case has a significant improvement immediately (the two cases start from the same initial condition) because mid- and high-frequency modes are overdamped. The residual response is from very low frequency modes that are not well damped by the control.

5 CONCLUSIONS

Active control is a potential enabler for future space telescopes with primary mirror areal densities an order of magnitude smaller than current generation telescopes, permitting an order of magnitude greater collecting area for the same launch weight. The reduced mass would be obtained by using very large numbers of identical small segments. Before such an architecture could be seriously considered for future missions, there are several challenges that must be overcome. A key challenge is the ability to control the resulting segment array, requiring control of thousands of degrees of freedom, with a comparable number of lightly-damped structural modes within the control bandwidth. Building off of recent research in controlling large flexible deformable mirrors, a control architecture for this problem is presented here; the approach combines collocated active damping with local position control.

First, real actuators and sensors have finite bandwidth, and thus any implementation of rate feedback to add damping will not be positive real above some frequency. However, there will always be some frequency at which the structure enters an “acoustic limit”, where the half-power bandwidth of any mode exceeds the modal spacing, and thus the phase excursions in the collocated transfer function decrease, due to multiple modes being simultaneously excited. It is precisely because there are many structural modes in this problem that this frequency is not unrealistically high, and hence practical active damping is stable provided it has a minimum bandwidth.

Second, in addition to the wide range of temporal frequencies, there is a wide range of spatial frequencies excited by any actuator. With collocated feedback, a global response pattern is generated in response to a local position error. A global feedback strategy could correct this behavior, but requiring information from the entire mirror has the potential to introduce robustness problems. Instead, a local control strategy is introduced that does not depend on model or state knowledge far away from a given actuator. This is derived not by considering what nearby information is necessary at each actuator location, but rather what

312 distribution of response is appropriate for any given local position error.

313 The strategy is demonstrated on a dynamic model of a 30 m mirror composed of 12 000
314 identical 30 cm diameter segments. The main conclusion is that the ability to control the
315 system is not a barrier to designing a space telescope with a large number of segments.

316 6 ACKNOWLEDGMENTS

317 The simulation code used here was developed by Mattias Björklund, of KTH, Sweden.

318 References

- 319 [1] M. Postman, T. Brown, K. Sembach, M. Giavalisco, W. Traub, K. Stapelfeldt,
320 D. Calzetti, W. Oegerle, R. M. Rich, H. P. Stahl, J. Tumlinson, M. Mountain, R. Soum-
321 mer, and T. Hyde, “Science drivers and requirements for an Advanced Technology Large
322 Aperture Space Telescope (ATLAST): Implications for technology development and
323 synergies with other future facilities,” in *Proc. SPIE Vol. 7731, Space Telescopes and
324 Instrumentation*, 2010.
- 325 [2] J. Nelson and G. H. Sanders, “The status of the Thirty Meter Telescope project,” in
326 *Proc. SPIE Vol. 7012, Ground-based and Airborne Telescopes II*, 2008.
- 327 [3] R. Gilmozzi and J. Spyromilio, “The 42m European ELT: status,” in *Proc. SPIE Vol.
328 7012, Ground-based and Airborne Telescopes II*, 2008.
- 329 [4] J. P. Gardner *et al.*, “The James Webb Space Telescope,” *Space Science Reviews*, vol.
330 123, pp. 485–606, 2006.
- 331 [5] D. C. Redding, G. S. Hickey, and S. C. Unwin, “Actuated mirrors for space telescopes,”
332 in *Proc. SPIE Vol. 7731, Space Telescopes and Instrumentation*, 2010.

- 333 [6] R. G. Dekany, D. G. MacMartin, G. A. Chanan, and M. Troy, “Advanced segmented
334 silicon space telescope (ASSiST),” in *Proc. SPIE Vol. 4849: Highly Innovative Space*
335 *Telescope Concepts*, 2002.
- 336 [7] K. Patterson, S. Pellegrino, and J. Breckinridge, “Shape correction of thin mirrors in
337 a reconfigurable modular space telescope,” in *Proc. SPIE Vol. 7731, Space Telescopes*
338 *and Instrumentation*, 2010.
- 339 [8] S. Padin, “Design considerations for a highly segmented mirror,” *Applied Optics*, vol. 42,
340 no. 16, pp. 3305–3312, 2003.
- 341 [9] W. R. Oegerle, L. R. Purves, J. G. Budinoff, R. V. Moe, T. M. Carnahan, D. C. Evans,
342 and C. K. Kim, “Concept for a large scalable space telescope: In-space assembly,” in
343 *Proc. SPIE Vol. 6265, Space Telescopes and Instrumentation I: Optical, Infrared, and*
344 *Millimeter*, 2006.
- 345 [10] M. J. Santer and K. A. Seffen, “Optical space telescope structures: The state of the art
346 and future directions,” *Aeronautical Journal*, vol. 113, no. 1148, pp. 633–645, 2009.
- 347 [11] D. G. MacMynowski, R. Heimsten, and T. Andersen, “Distributed force control of
348 deformable mirrors,” *European J. Control*, 2011.
- 349 [12] R. Heimsten, M. Owner-Petersen, T. Andersen, and D. G. MacMynowski, “Distributed
350 force control of deformable mirrors,” *submitted, Optical Engineering*, 2011.
- 351 [13] W. Doggett, “Robotic assembly of truss structures for space systems and future research
352 plans,” in *IEEE Aerospace Conference Proceedings*, 2002.
- 353 [14] J. Watson, T. Collins, and H. Bush, “A history of astronaut construction of large
354 space structures at NASA Langley Research Center,” in *IEEE Aerospace Conference*
355 *Proceedings*, 2002.

- 356 [15] J. H. Burge, E. Sabatke, J. R. P. Angel, and N. J. Woolf, “Optical design of giant
357 telescopes for space,” in *Proc. SPIE Vol. 4092, Novel Optical Systems Design and Op-*
358 *timization III*, 2000.
- 359 [16] G. Chanan, D. G. MacMartin, J. Nelson, and T. Mast, “Control and alignment of
360 segmented-mirror telescopes: Matrices, modes, and error propagation,” *Applied Optics*,
361 vol. 43, no. 6, pp. 1223–1232, 2004.
- 362 [17] D. G. MacMynowski, “Interaction matrix uncertainty in active (and adaptive) optics,”
363 *Applied Optics*, vol. 48, no. 11, pp. 2105–2114, 2009.
- 364 [18] —, “Hierarchic estimation for control of segmented-mirror telescopes,” *AIAA J. Guid-*
365 *ance, Control and Dynamics*, vol. 28, no. 5, 2005.
- 366 [19] L. Lessard, M. West, D. MacMynowski, and S. Lall, “Warm-started wavefront recon-
367 struction for adaptive optics,” *J. Optical Society of America, A*, vol. 25, no. 5, pp.
368 1147–1155, 2008.
- 369 [20] D. G. MacMartin, “Local, hierarchic, and iterative reconstructors for adaptive optics,”
370 *J. of the Optical Society of America, A*, vol. 20, no. 6, pp. 1084–1093, 2003.